

Inhibition Effect of 1-vinyl-3-ethylimidazolium Bromide for X65 Steel in 0.5 M Sulfuric Acid Solution

Nanxi Chen, Shengtao Zhang^{}, Yujie Qiang, Shenyong Xu, Xiaolei Ren*

School of Chemistry and Chemical Engineering, Chongqing University, Chongqing 400044, P.R. China

^{*}E-mail: stzhang_cqu@163.com

Received: 20 May 2016 / Accepted: 19 June 2016 / Published: 7 July 2016

The corrosion inhibitive effect of 1-vinyl-3-ethylimidazolium bromide ([VEIM]Br) for X65 steel in 0.5 M H₂SO₄ solution has been investigated through electrochemical tests, weight loss, scanning electronic microscopy (SEM) and quantum chemical calculation. The electrochemical and weight loss results revealed that 1-vinyl-3-ethylimidazolium bromide acted as a modest cathodic inhibitor and the inhibition efficiency was up to 85% when the concentration of inhibitor reached 10 mM. SEM observation showed obviously the protection effect using the ionic liquid. The adsorption of [VEIM]Br molecule on the X65 steel surface was found to obey the Langmuir adsorption isotherm. The quantum chemical calculations and molecular dynamics simulation appeared that [VEIM]Br was adsorbed strongly on the X65 steel surface.

Keywords: X65 steel, Corrosion inhibition, Ionic liquids, Electrochemical tests, Theoretical study

1. INTRODUCTION

Steel pipelines have been employed in mass amounts in petroleum production, natural gas processing and coal mining throughout the world[1-3]. Corrosion is a byproduct inevitably in these industries. Special attention should be paid to handle this problem because the corrosion can lead leakage of liquid and gas, and the reinstatement work is time-consuming and cost[2, 4-7]. Acid picking[8-10] is often used to get rid of the corrosion and the addition of inhibitor is provided to mitigate acid attack. In general, the application of inhibitor is one of the most practical and economic methods to prevent the corrosion for metal in acid solution[5, 8-12]. The organic inhibitors, which consist of heteroatoms, such as nitrogen, phosphorous, oxygen, triple bonds, aromatic rings and imine(–C=C–) functional groups[13-15] are always effective for corrosion protection. These molecules

affect by forming an adsorption film and blocking the corrosion active sites on the metal surface[16, 17].

Nowadays, since the application of toxic and expensive inhibitor becomes restricted, more and more eco-friendly and nontoxic substance are investigated as corrosion inhibitor[2, 18-21]. Ionic liquids (ILs) have been employed in batteries[22], electrolyte[23], polymer science[24] and a wide range of fields due to its unique physical and chemical characteristics which are low vapor pressure, stable thermal ability, good solubility and low melting point[25]. Ionic liquids[26] is a kind of molten salt at room temperature ($\leq 100^{\circ}\text{C}$) and usually comprised of organic compounds as cation and inorganic one as anion. It is worthy to say that the different combination of anion and cation provide the possibility of more effective inhibitor[10, 27-32]. However, the number of researches about ionic liquids as corrosion inhibitor is relatively limited.

The aim of this work is to study the inhibition action of 1-vinyl-3-ethylimidazolium bromide ([VEIM]Br) for X65 steel in 0.5 M H_2SO_4 solution using measurements of potentiodynamic polarization, electrochemical impedance spectroscopy (EIS), weight loss and scanning electronic microscope (SEM). In addition, quantum chemical calculations and molecular dynamic simulation are applied to investigate the active sites and adsorption properties of [VEIM]Br on X65 steel surface.

2. EXPERIMENTAL

2.1. Materials and samples preparation

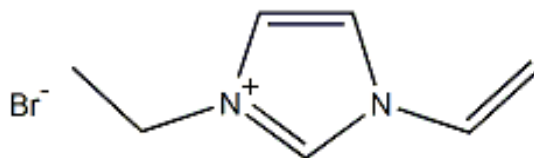


Figure 1. Molecular structure of 1-vinyl-3-ethylimidazolium bromide

The composition of the material X65 was Si (0.17%), Mn (1.64%), Cr (0.16%), Nb (0.041%), C (0.06%), Al (0.035%) and the remainder Fe. The experimental inhibitor 1-vinyl-3-ethylimidazolium bromide ([VEIM]Br as shown in fig.1) was purchased from Lanzhou Greenchem ILs, LICP. CAS. China with the purity of 99% and was used as received. The corrosion medium was 0.5 M H_2SO_4 solution which was made of appropriate sulfuric acid and distilled water. The corrosion tests were performed in 0.5 M H_2SO_4 solution with various concentrations (1-10 mM) of [VEIM]Br, and the one without the inhibitor was treated as blank for comparison. The size of specimens for weight loss experiments were 2 cm \times 2 cm \times 1 cm, while the ones for electrochemical measurements and surface analysis were 1 cm \times 1 cm \times 1 cm and 0.5 cm \times 0.5 cm \times 0.5 cm, respectively. Prior to each measurement, the specimens were abraded painstakingly using emery papers (400 to 2000 grit), then rinsed with distilled water, degreased in acetone ultrasonically and dried at room temperature lastly. All the experiments were open to the air and performed using aqueous thermostat bath at 298 ± 1 K.

2.2. Weight loss measurements

X65 samples for each inhibitor concentration were prepared in triplicate and weighted precisely, after that they were suspended in 0.5 M H₂SO₄ solution containing different concentration of [VEIM]Br for 24 h at 298 K. Then the specimens were taken out and descaled by being scrubbed with a soft brush, and infused in the rust removal solution combined with 20% NaOH and Zn powders. Afterwards, they were cleaned by distilled water and acetone successively, and dried at room temperature before being weighted. A series of average values of the weight loss data and immersion time were used to calculate the mean corrosion rates.

2.3. Electrochemical measurements

A conventional three electrode cell system[33] was used for electrochemical measurements which were carried out using CHI 660D electrochemical workstation. A saturated calomel electrode (SCE) with a luggin capillary was the reference electrode (RE), the X65 steel was worked as the working electrode (WE) with a contact area of 1 cm², a platinum electrode was the counter electrode (CE). All potential values in this study were referred to the SCE. The electrodes were allowed to be soaked in the test medium for 40 min until a steady-state open circuit potential (E_{OCP}) was reached.

Potentiodynamic electrochemical polarization curves were acquired by setting the electrode potential range of ± 250 mV versus OCP with 2 mV s⁻¹ scan rate.

Electrochemical impedance spectroscopy (EIS) measurements were carried out in frequency range from 100 kHz to 10 mHz at the open circuit potential (OCP), and 5 mV amplitude as the excitation signal was used to perturb the system.

2.4. Morphological characterization

After immersion in 0.5 M H₂SO₄ solution without and with addition of 10 mM inhibitor at 298 K for 6 h, the surface morphologies of these specimens were examined by scanning electron microscopy (SEM) instrument. The size of test surface was 0.25 cm². All micrographs were taken at a magnification power ($\times 800$).

2.5. Calculation methods

Quantum chemical calculations were employed by Gaussian 03W software. The [VEIM]Br molecule was fully optimized by density functional theory (DFT) using B3LYP functional with 6-311++G (d,p) basis set. The key quantum chemical parameters including the energy of highest occupied molecular orbital (E_{HOMO}), the energy of lowest unoccupied molecular orbital (E_{LUMO}), energy gap ($\Delta E = E_{LUMO} - E_{HOMO}$) and dipole moment (μ) were calculated and discussed.

The molecular dynamics simulations of the interaction between [VEIM]Br and the Fe (110) surface were carried out by the discover module in Material Studio 6.0 software with NVT ensemble, 298 K, a time step of 1 fs and simulation time of 1000 ps.

3. RESULTS AND DISCUSSION

3.1. Potentiodynamic polarization test

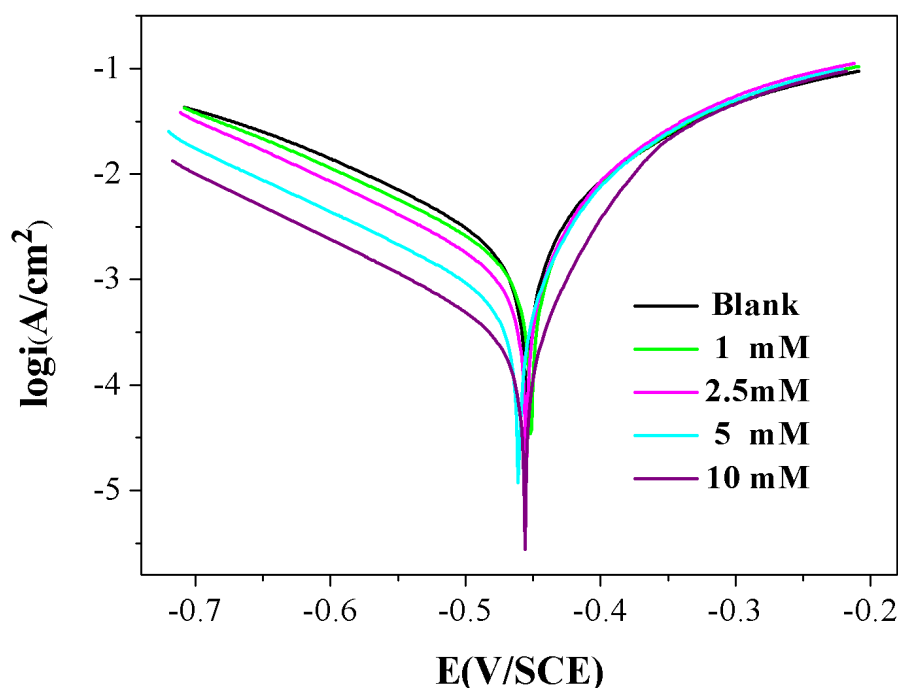


Figure 2. Polarization curves for X65 steel in 0.5 M H₂SO₄ solution with different concentrations of [VEIM]Br

Table 1. The Potentiodynamic polarization parameters for X65 steel in 0.5 M H₂SO₄ solution in the absence and presence of different concentrations of [VEIM]Br

C (mM)	E_{corr} (mV)	i_{corr} (mA cm ⁻²)	β_c (mV dec ⁻¹)	β_a (mV dec ⁻¹)	$\eta\%$
0	-455	1.964	154.4	124.4	/
1	-452	1.526	157.2	114.6	22.30
2.5	-455	1.096	151.3	114.6	44.20
5	-461	0.6069	153.5	103.3	69.10
10	-456	0.2756	147.6	48.7	85.97

The potentiodynamic polarization curves for X65 steel in 0.5 M H₂SO₄ solution with and without various concentrations of the inhibitor [VEIM]Br at 298 K are shown in Fig. 2. Extrapolation

method[11] is used to determine the polarization parameters which are corrosion potential (E_{corr}), corrosion current density (I_{corr}), cathodic and anodic Tafel slope (β_c and β_a), and the percentage inhibition efficiency (η). The values above all are listed in Table 1. The inhibition efficiency η is calculated by the following equation:

$$\eta = \frac{i_{\text{corr}}^0 - i_{\text{corr}}}{i_{\text{corr}}^0} \times 100 \quad (1)$$

Where i_{corr}^0 and i_{corr} are uninhibited and inhibited corrosion current densities, respectively. Inspection of the Fig. 2 reveals that the cathodic polarization curves are changed to lower current densities with increasing inhibitor concentration, but no significant decrease in anodic current density until the concentration adds up to 10 mM. It indicates that [VEIM]Br in 0.5 M H_2SO_4 solution mainly retards the hydrogen ions reaction on the cathodic region, so it acts as a modest cathodic inhibitor as well as not much of anodic inhibitor. Also, it is clear that the addition of inhibitor causes negative shift in E_{corr} when compared with that of the blank and the displacement of E_{corr} is less than 20 mV, which suggests that the inhibitor is a mixed type inhibitor with a predominantly cathodic action. Furthermore, the cathodic polarization curves of different inhibitor concentrations tend to be almost paralleled, indicating that the retardation of the cathodic ions affects without changing the mechanism of hydrogen reduction which is actually activation- controlled[28].

From the Table 1, it can be seen that the corrosion current densities decrease substantially, causing the increase of the inhibition efficiency. The η reaches a maximum values with 85% when the concentration of inhibitor up to 10 mM. Furthermore, both of β_c and β_a do not change largely, which demonstrates that [VEIM]Br acts as a mixed type inhibitor and absorbed to the steel surface without modifying the mechanism in the process[4].

3.2. Electrochemical impedance spectroscopy (EIS)

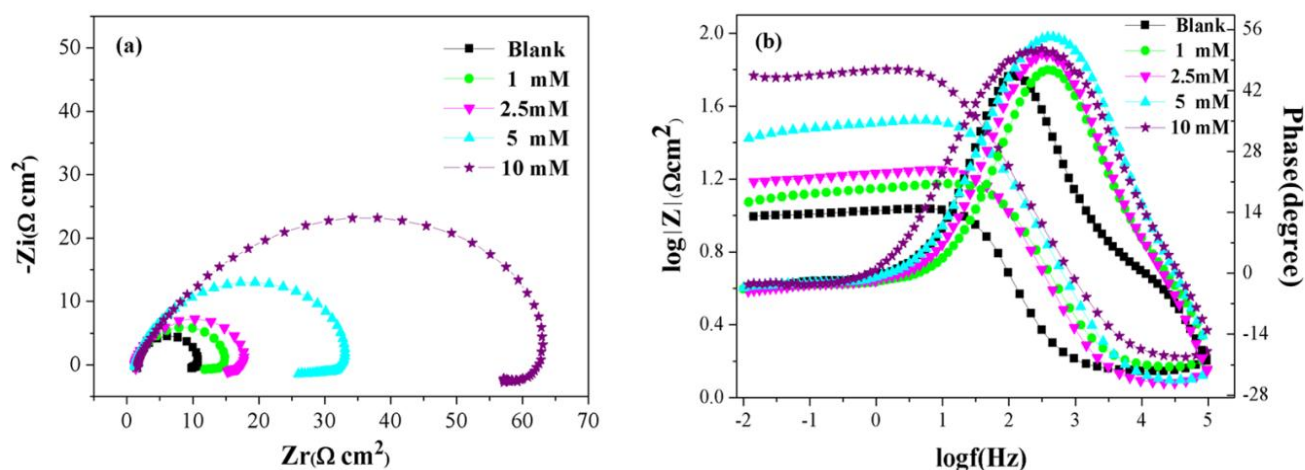


Figure 3. Nyquist and Bode plots for X65 steel in 0.5 M H_2SO_4 solution with different concentrations of [VEIM]Br

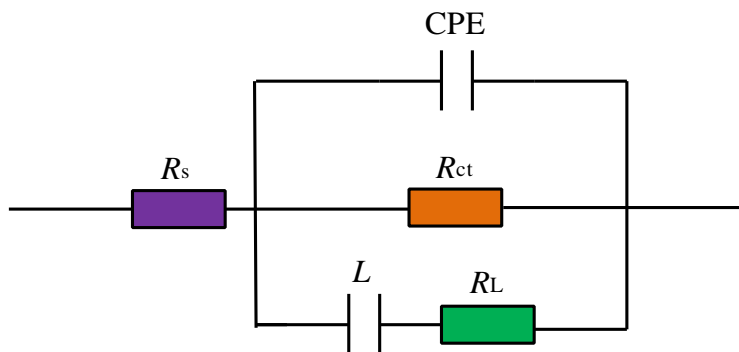


Figure 4. Equivalent electron circuit model

Table 2. Impedance parameters of X65 steel in 0.5 M H₂SO₄ solution in the absence and presence of different concentrations of [VEIM]Br

C (mM)	R_s ($\Omega \text{ cm}^2$)	CPE		C_{dl} ($\mu\text{F cm}^{-2}$)	R_{ct} ($\Omega \text{ cm}^2$)	L ($\Omega \text{ cm}^2$)	R_L ($\Omega \text{ cm}^2$)	η (%)
		$Y_0 (\times 10^{-6} \text{ S s}^n \text{ cm}^{-2})$	n					
0	1.465	482.4	0.95	363.2	9.52	37.58	80.43	/
1	1.515	178.4	0.91	100.1	13.28	36.66	65.19	28.3
2.5	1.273	224.2	0.90	122.0	16.57	48.20	107.3	42.5
5	1.250	201.3	0.85	85.93	32.20	139.9	169.2	70.4
10	1.644	335.4	0.76	108.6	65.60	168.6	387.7	85.5

Fig. 3a and Fig. 3b show the Nyquist and Bode plots for X65 steel in 0.5 M H₂SO₄ solution containing different concentrations of [VEIM]Br at 298 K. Nyquist plots can be regarded as two parts. The one is a capacitive loop at high frequency, which is related to the time constant of charge transfer in the corrosion process resistance and double layer behavior. The another is an inductive loop at low frequency, which is related to the relaxation process of adsorbed species, such as (SO₄²⁻)_{ads} and (H⁺)_{ads} or re-dissolution of the working electrode surface. The capacitive loop present depressed semicircle, which is often due to the frequency dispersion resulted from the heterogeneousness and roughness of the electrode surface[12]. It is obvious that the shape of the Nyquist plots almost keep the same with different concentrations of inhibitor, suggesting that the addition of [VEIM]Br has change the corrosion mechanism slightly and the main controlled factor of corrosion process is charge-transfer[34]. Fig. 3a presents the diameters of the capacitive loops increase upon increasing inhibitor concentration and are larger than the one in blank solution, while the same phenomenon is inspected from the Bode plots in Fig. 3b. This behavior indicates that the inhibitor takes the place of water behind the metal surface and adsorbed on the X65 steel surface, which causes the difficulty of the charge-transfer, leading the increase of inhibition efficiency.

From the impedance spectra analysis, the equivalent circuit (EC) shown in Fig.4 are determine to simulate the EIS results by using ZSimpwin software. The corresponding data are listed in Table 2. The employed circuit consists of solution resistance (R_s), constant phase element (CPE), charge

transfer resistance (R_{ct}), inductive elements L and R_L . The constant phase element is often used to take the place of a pure capacitor and can be expressed as follows[6]:

$$Z_{CPE} = \frac{1}{Y(j\omega)^n} \quad (2)$$

Where Y is the CPE constant, j is the imaginary number ($j^2=-1$), ω is the angular frequency ($\omega=2\pi f$), and n is the phase shift related to the inhomogeneity on the steel surface. The double layer capacitance C_{dl} which is deduced by the equation[35]:

$$C_{dl} = Y(\omega)^{n-1} = Y(2\pi f_{z_{im-Max}})^{n-1} \quad (3)$$

Where ω is the angular frequency when the imaginary part of the impedance spectrum reach the maximum value. The results obtained in Table 2 show that R_{ct} increases from $9.52 \Omega \text{ cm}^2$ to $65.6 \Omega \text{ cm}^2$ in the blank and 10 mM inhibitor solution, respectively. Conversely, the double layer capacitances are all smaller than the blank one[36]. Thus, the η value increases from 28.3% in the 1 mM [VEIM]Br to 85.8% in the 0.5 M H_2SO_4 solution containing 10 mM [VEIM]Br. The inhibition efficiency is obtained through the following equation:

$$\eta = \frac{R_{ct} - R_{ct}^0}{R_{ct}} \times 100 \quad (4)$$

Where R_{ct} and R_{ct}^0 are the charge transfer resistance values with and without [VEIM]Br, respectively. It is glad to say that the results of polarization agree with the ones that of EIS measurements, demonstrating that [VEIM]Br affects significant inhibition in 0.5 M H_2SO_4 solution.

3.3. Weight loss measurements

Table 3. Corrosion parameters for X65 in 0.5 M H_2SO_4 containing different concentrations of [VEIM]Br for 24 h at 298 K

C (mM)	v ($\text{g m}^{-2} \text{ h}^{-1}$)	$\eta\%$	θ
0	24.34	/	/
1	18.81	22.72	0.2272
2.5	14.53	40.30	0.4030
5	10.14	58.33	0.5833
10	4.16	82.91	0.8291

The weight loss data of X65 in 0.5 M H_2SO_4 solution in the absence and presence of different concentrations of inhibitor for 24 h at 298 K are listed in Table 3. The inhibition efficiency (η) and surface coverage (θ) are calculated as follows:

$$\eta = \frac{v^0 - v}{v^0} \times 100 \quad (5)$$

$$\theta = \frac{v^0 - v}{v^0} \quad (6)$$

Where v^0 and v are the corrosion rates without and with [VEIM]Br in 0.5 M H_2SO_4 solution, respectively. Table 3 shows that v decrease upon increasing inhibitor concentration, causing the increase of inhibition efficiency. The results can be explained by the adsorption of [VEIM]Br, which causes the increase of surface coverage[37]. Also, the weight loss results and the electrochemical experiments are in the same trend but not coincide with each other very well.

3.4. Adsorption isotherm

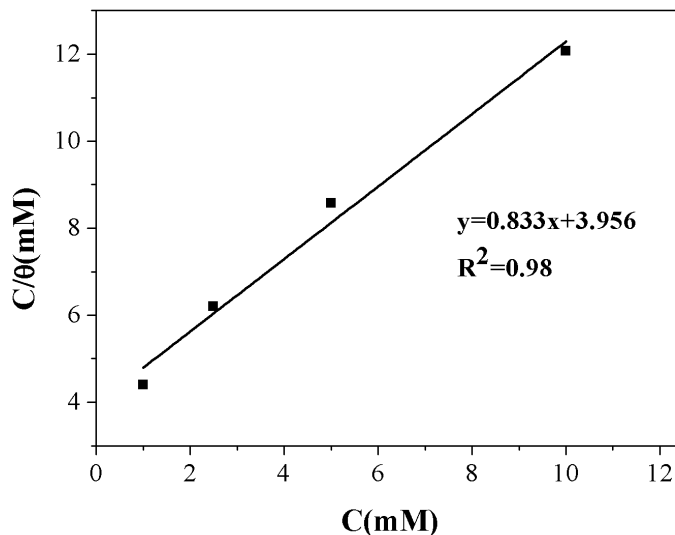


Figure 5. Langmuir adsorption isotherm of [VEIM]Br on the surface of X65 steel in 0.5 M H₂SO₄ solution

It is known that the corrosion inhibition process is due to the adsorption on the metal-solution interface. To describe the information of the interaction between the X65 steel and [VEIM]Br, several typical adsorption isotherms such as El-Awady, Temkm, Langmuir, Frumkin are assessed to fit our results[17, 38, 39]. Notably, Langmuir adsorption isotherm is found to be the best description of the adsorption behavior of [VEIM]Br.

$$\frac{C}{\theta} = \frac{1}{K_{ads}} + C \tag{7}$$

Here, *C* is the concentration of inhibitor, *θ* is the degree surface coverage which is given in weight loss measurements and *K_{ads}* is the equilibrium constant of adsorption process and is related to the free energy of adsorption(ΔG_{ads}^0):

$$K_{ads} = \frac{1}{55.5} \exp\left(\frac{-\Delta G_{ads}^0}{RT}\right) \tag{8}$$

Here, 55.5 is the concentration of water in the solution (mol L⁻¹), *R* is the molar gas constant (8.314 J mol⁻¹K⁻¹) and *T* is the absolute temperature (K). From Fig. 5, a straight line with the coefficient (*R*²=0.98) is obtained, showing the relationship between *C* and *C/θ*. The negative value of ΔG_{ads}^0 (-23.66 KJ mol⁻¹) ensures that the inhibitor adsorption is a spontaneous process. Generally, the values of ΔG_{ads}^0 higher than -20 kJ mol⁻¹ are consistent with physical adsorption due to the electrostatic interaction between the charged inhibitor molecules and the charged metal. While the ΔG_{ads}^0 values lower than -40 kJ mol⁻¹ are considered involving as chemical adsorption which is attributed to the coordinated type of bond formed by sharing or transfer electron. Since the value of ΔG_{ads}^0 in our studies is between -20 kJ/mol and -40 kJ/mol, we can conclude the adsorption mechanism is consist of both physisorption and chemisorption[40].

3.5. Surface morphology

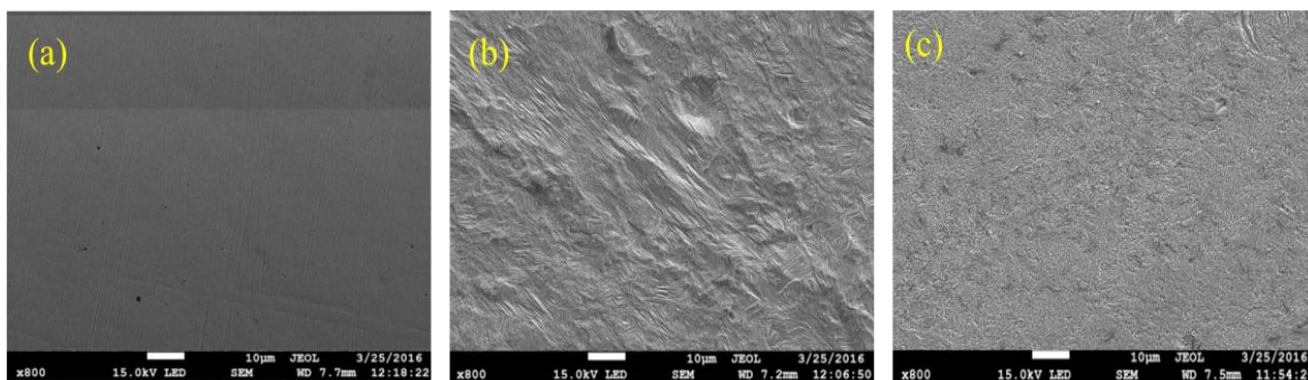


Figure 6. SEM micrographs of freshly polished specimen (a) and the specimens immersed in 0.5 M H_2SO_4 solution for 6 h without [VEIM]Br (b), with 10 mM [VEIM]Br (c)

The scanning electron microscope images of the X65 steel surface are recorded in Fig.6. The freshly polished specimen (Fig. 6a) shows smooth flat surface of the X65 steel. On the contrary, after immersion in 0.5 M H_2SO_4 solution for 6 h at 298 K, the surface appears heavy damages (Fig. 6b), such as the rough surface layers and corrosion cavities. However, in the presence of 10 mM [VEIM]Br (Fig. 6c), the steel surface is slightly damaged and exhibits a neat surface comparatively. The result enhances the [VEIM]Br is an effective inhibitor for X65 steel in 0.5 M H_2SO_4 solution.

3.6. Quantum chemical calculations

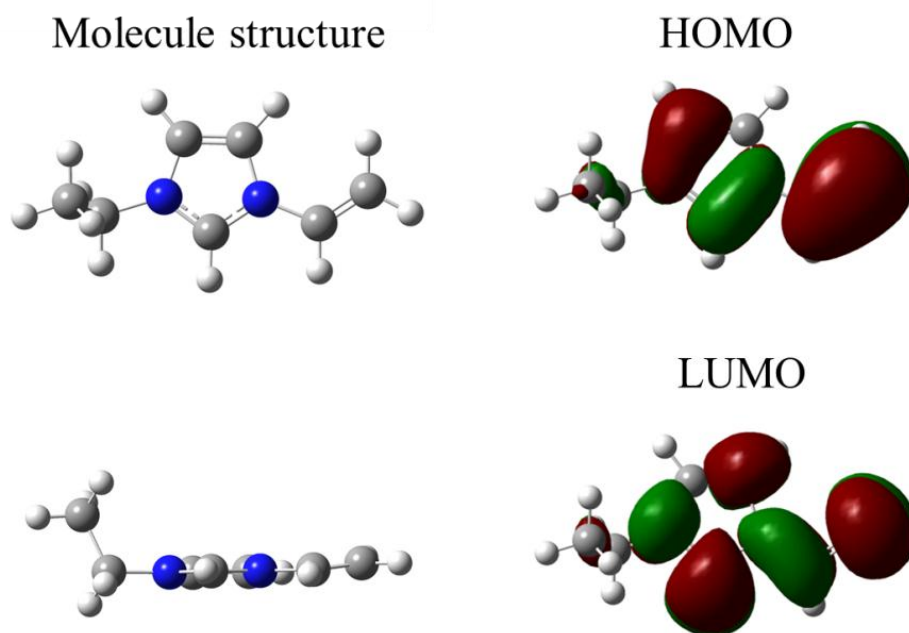


Figure 7. Optimized geometric structures and the distributions of HOMO and LUMO for [VEIM]Br cation

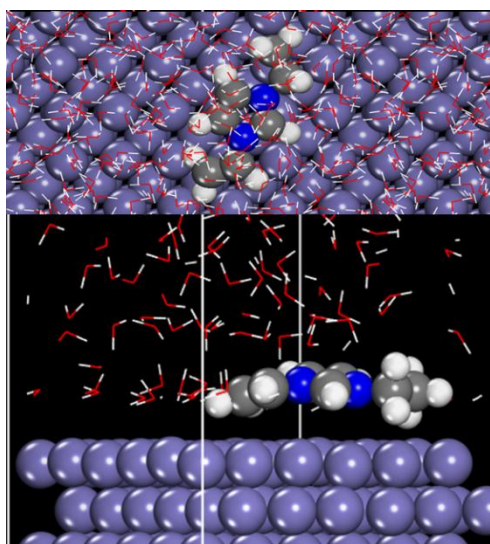
Table 4. Quantum chemical parameters for the VEIM cation

E_{HOMO} (eV)	E_{LUMO} (eV)	ΔE (eV)	μ (D)
-11.51	-5.70	5.81	0.6351

Quantum chemical calculations play an important role towards the studies of design and development of organic inhibitors in corrosion field[5, 41]. Notably, in order to study the adsorption and inhibition mechanism which are related to the structure of the inhibitor molecular and its inhibiting effect, density functional theory (DFT) has been conducted. The full optimized minimum energy geometrical configuration and the frontier molecule orbital density distributions of [VEIM]Br are shown in Fig. 7, whereas the calculated quantum chemical parameters including E_{LUMO} , E_{HOMO} , ΔE , and μ are given in Table 4.

From the Fig. 7 we can see that the HOMO and LUMO energy orbitals are mostly occupied on the heteroatoms in imidazole and the double bond. According to the frontier molecular orbital theory, E_{HOMO} is often relevant to the ability of the molecule to donate electrons, and a high value of E_{HOMO} indicates the tendency of organic molecules to donate electrons to acceptor molecules. E_{LUMO} is related to the ability of the molecule to accept electrons and the lower value of E_{LUMO} shows the easier acceptance of electrons from the metal surface[15, 42]. The energy gap is generally associated with chemical reactivity, so the molecule with lower ΔE value has higher inhibition efficiency for metal corrosion. Besides, it was reported previously that high dipole moment (μ) are responsible for enhancing the inhibition efficiency. Remarkably, the low value of ΔE and high value of μ are shown in table 4, indicating a favorable inhibitive ability of [VEIM]Br. These observations are in good agreement with the experimental results of the present work.

3.7. Molecular dynamic simulation

**Figure 8.** Equilibrium adsorption configurations of [VEIM]Br on X65 steel in 0.5 M H₂SO₄ solution

The top view and side view of the equilibrium configuration of the inhibitor adsorbed on the Fe (110) surface are shown in Figure 8. It is clear that the [VEIM]Br is nearly parallel with the Fe (110) surface through the imidazole ring. This parallel mode can enlarge the contact area between [VEIM]Br molecules and surface of X65 steel and minimize the damage from the corrosive media. The value of interaction energy obtained from the molecular dynamics simulation is -380.01 kJ/mol. The high negative value demonstrates the strong adsorption between [VEIM]Br and the X65 steel surface[43, 44]. Besides, the inhibitor molecules show high inhibition p electron interactions between the X65 steel surface and the imidazole ring. So the [VEIM]Br adsorption system is stable and therefore exhibits an effective protection ability.

4. CONCLUSIONS

[VEIM]Br presents good inhibition for corrosion of X65 steel in 0.5 M H_2SO_4 solution at 298 K, and the inhibition efficiency increase with concentration of [VEIM]Br. The Tafel polarization curves show that [VEIM]Br in 0.5 M H_2SO_4 solution is a mixed-type inhibitor and mainly retard the hydrogen ions reaction on the cathodic region. The adsorption of the inhibitors on the X65 steel obeys Langmuir isotherm model with a mixed physisorption and chemisorption. The inhibition efficiency determined from polarization and EIS results are in accordance with the weight loss measurements. The SEM images show a protective surface compared to the corrosive one, which indicates that [VEIM]Br is an effective inhibitor for X65 steel in 0.5 M H_2SO_4 solution. Finally, quantum chemical calculations and molecular dynamic simulation give a favorable support for the experimental results.

ACKNOWLEDGMENTS

This research was supported by Natural Science Foundation of China (No. 21376282).

Reference

1. A. A. Farag, M. A. Hegazy. *Corrosion Science*, 74 (2013) 168.
2. E. Sadeghi Meresht, T. Shahrabi Farahani, J. Neshati. *Corrosion Science*, 54 (2012) 36.
3. E. Sadeghi Meresht, T. Shahrabi Farahani, J. Neshati. *Engineering Failure Analysis*, 18 (2011) 963.
4. F. Y. Cui, L. Guo, S. T. Zhang. *Materials and Corrosion*, 65 (2014) 1194.
5. L. Guo, S. Zhu, S. Zhang, Q. He, W. Li. *Corrosion Science*, 87 (2014) 366.
6. S. Tu, X. Jiang, L. Zhou, M. Duan, H. Wang, X. Jiang. *Corrosion Science*, 65 (2012) 13.
7. Y. H. Qibo Zhang, Zhongren Zhou. *International Journal of Electrochemical Science*, 8 (2013) 10239
8. D. Guzmán-Lucero, O. Olivares-Xometl, R. MartíNez-Palou, N. V. Likhanova, M. A. DomíNquez-Aguilar, V. Garibay-Febles. *Industrial & Engineering Chemistry Research*, 50 (2011) 7129.
9. M. A. Hegazy, A. M. Badawi, S. S. Abd El Rehim, W. M. Kamel. *Corrosion Science*, 69 (2013) 110.
10. Q. B. Zhang, Y. X. Hua. *Electrochimica Acta*, 54 (2009) 1881.
11. Y. Qiang, S. Zhang, S. Xu, L. Yin. *RSC Adv*, 5 (2015) 63866.
12. S. A. Umoren, Y. Li, F. H. Wang. *Corrosion Science*, 52 (2010) 2422.

13. L. O. Olasunkanmi, I. B. Obot, M. M. Kabanda, E. E. Ebenso. *The Journal of Physical Chemistry C*, 119 (2015) 16004.
14. L. Liu, Y. Zhang, X. Yin, J. Qian. *Surface and Interface Analysis*, 45 (2013) 949.
15. S. Z. Yujie Qiang, Shenyang Xu, Lei Guo, Nanxi Chen, Ime B. Obot. *International Journal of Electrochemical Science*, 11 (2016) 3147
16. S. Zhang, Z. Tao, S. Liao, F. Wu. *Corrosion Science*, 52 (2010) 3126.
17. A. Popova, M. Christov, S. Raicheva, E. Sokolova. *Corrosion Science*, 46 (2004) 1333.
18. M. A. Migahed, A. A. Farag, S. M. Elsaed, R. Kamal, M. Mostfa, H. A. El-Bary. *Materials Chemistry and Physics*, 125 (2011) 125.
19. M. A. Hegazy, M. Abdallah, H. Ahmed. *Corrosion Science*, 52 (2010) 2897.
20. A. M. Fekry, M. A. Ameer. *International Journal of Hydrogen Energy*, 35 (2010) 7641.
21. A. Khamis, M. M. Saleh, M. I. Awad, B. E. El-Anadouli. *Journal of advanced research*, 5 (2014) 637.
22. S. Pandian, S. G. Raju, K. S. Hariharan, S. M. Kolake, D.-H. Park, M.-J. Lee. *Journal of Power Sources*, 286 (2015) 204.
23. M. Galiński, A. Lewandowski, I. Stępnia. *Electrochimica Acta*, 51 (2006) 5567.
24. J. Lu, F. Yan, J. Texter. *Progress in Polymer Science*, 34 (2009) 431.
25. M. Petkovic, K. R. Seddon, L. P. Rebelo, C. Silva Pereira. *Chemical Society reviews*, 40 (2011) 1383.
26. T. Torimoto, T. Tsuda, K. Okazaki, S. Kuwabata. *Advanced materials*, 22 (2010) 1196.
27. E.-S. Sherif, H. Abdo, S. Abedin. *Materials*, 8 (2015) 3883.
28. X. Zheng, S. Zhang, W. Li, M. Gong, L. Yin. *Corrosion Science*, 95 (2015) 168.
29. X. Zheng, S. Zhang, W. Li, L. Yin, J. He, J. Wu. *Corrosion Science*, 80 (2014) 383.
30. X. Zhou, H. Yang, F. Wang. *Electrochimica Acta*, 56 (2011) 4268.
31. O. Olivares-Xometl, C. López-Aguilar, P. Herrasti-González, N. V. Likhanova, I. Lijanová, R. Martínez-Palou, et al. *Industrial & Engineering Chemistry Research*, 53 (2014) 9534.
32. L. C. M. Sudhish K. Shukla, Eno E. Ebenso. *International Journal of Electrochemical Science*, 6 (2011) 4286
33. M. A. Hegazy, A. A. Nazeer, K. Shalabi. *Journal of Molecular Liquids*, 209 (2015) 419.
34. G. a. E.-M. Ayman M. Atta, Hamad A. Allohedan1 and Mahmood M. S. Abdullah. *International Journal of Electrochemical Science*, 10 (2015) 6106
35. X. Zheng, S. Zhang, M. Gong, W. Li. *Industrial & Engineering Chemistry Research*, 53 (2014) 16349.
36. Y. Qiang, S. Zhang, S. Xu, W. Li. *Journal of colloid and interface science*, 472 (2016) 52.
37. M. K. Pavithra, T. V. Venkatesha, K. Vathsala, K. O. Nayana. *Corrosion Science*, 52 (2010) 3811.
38. E. E. Oguzie, Y. Li, S. G. Wang, F. Wang. *RSC Advances*, 1 (2011) 866.
39. G. a. E.-M. Ayman M. Atta1, Hamad A. Allohedan , and Mahmood M. S. Abdullah. *International Journal of Electrochemical Science*, 10 (2015).
40. M. M. Solomon, S. A. Umoren, I. I. Udosoro, A. P. Udoh. *Corrosion Science*, 52 (2010) 1317.
41. A. N. Majid Khodaei-Tehrani. *International Journal of Electrochemical Science*, 10 (2015) 6855
42. H. S. M. Belayachi, A. El Assry, H. Oudda, S. Boukhris, M. Ebn Touhami. *International Journal of Electrochemical Science*, 10 (2015) 3038
43. B. Xu, Y. Ji, X. Zhang, X. Jin, W. Yang, Y. Chen. *Journal of the Taiwan Institute of Chemical Engineers*, 59 (2016) 526.
44. A. Dutta, S. K. Saha, P. Banerjee, D. Sukul. *Corrosion Science*, 98 (2015) 541.